Faraday Discussions

Accepted Manuscript

This manuscript will be presented and discussed at a forthcoming Faraday Discussion meeting. All delegates can contribute to the discussion which will be included in the final volume.

Register now to attend! Full details of all upcoming meetings: http://rsc.li/fd-upcoming-meetings

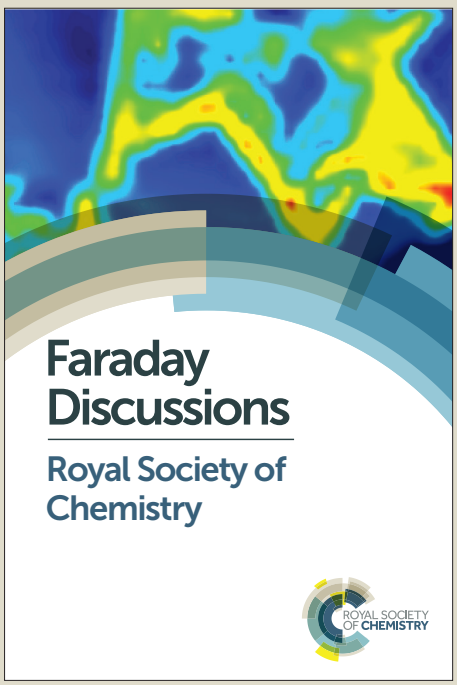

This is an *Accepted Manuscript*, which has been through the Royal Society of Chemistry peer review process and has been accepted for publication.

Accepted Manuscripts are published online shortly after acceptance, before technical editing, formatting and proof reading. Using this free service, authors can make their results available to the community, in citable form, before we publish the edited article. We will replace this *Accepted Manuscript* with the edited and formatted *Advance Article* as soon as it is available.

You can find more information about *Accepted Manuscripts* in the Information for Authors.

Please note that technical editing may introduce minor changes to the text and/or graphics, which may alter content. The journal's standard Terms & Conditions and the Ethical guidelines still apply. In no event shall the Royal Society of Chemistry be held responsible for any errors or omissions in this *Accepted Manuscript* or any consequences arising from the use of any information it contains.

ROYAL SOCIETY OF CHEMISTRY

www.rsc.org/faraday_d

Membrane-Mediated Aggregation of Anisotropically Curved Nanoparticles *

Alexander D. Olinger and Eric J. Spangler
Department of Biomedical Engineering, The University of Memphis, Memphis, TN 38152, USA and Department of Physics and Materials Science, The University of Memphis, Memphis, TN 38152

P.B. Sunil Kumar †
Department of Physics, Indian Institute of Technology Madras, Chennai - 600 036, India

Mohamed Laradji ‡
Department of Physics and Materials Science, The University of Memphis, Memphis, TN 38152, USA

Using systematic numerical simulations, we study the self-assembly of elongated curved nanoparticles on lipid vesicles. Our simulations are based on molecular dynamics of a coarse-grained implicit-solvent model of self-assembled lipid membranes with a Langevin thermostat. Here we consider only the case wherein nanoparticle-nanoparticle interaction is repulsive, only the concave surface of the nanoparticle interacts attractively with the lipid head groups and only the outer surface of the vesicle is exposed to the nanoparticles. Upon their adhesion on the vesicle, the curved nanoparticles generate local curvature on the membrane. The resulting nanoparticles-generated membrane curvature leads in turn to the nanoparticles self-assembly into two main types of aggregates corresponding to chain aggregates at low adhesion strengths and aster aggregates at high adhesion strength. The chain-like aggregates are due to the fact that at low values of the adhesion strength, the nanoparticles prefer to lie parallel to each other. As the adhesion strength is increased, a splay angle between the nanoparticles is induced with a magnitude that increases with increasing adhesion strength. The origin of the splay angles between the nanoparticles is shown to be saddle-like membrane deformations induced by a tilt of the lipids around the nanoparticles. This phenomenon of membrane mediated self-assembly of anisotropically curved nanoparticles is explored for systems with varying nanoparticles number densities, adhesion strength, and nanoparticles intrinsic curvature.

I. INTRODUCTION

Matrix assisted assembly of nanomaterials can be achieved through their mixing with liquid crystals [1], block copolymers [2], or simply as a result of their aggregation at fluid-fluid interfaces [3]. The self-assembly of colloidal and nanoscale particles at fluid-fluid interfaces, in particular, is driven by the wetting properties of the particle at the interface, which is controlled in part by the interfacial tension of the coexisting fluids. Stable self-assemblies of small nanoparticles at fluid-fluid interfaces tend however to be dynamic and lack long-range order [4]. Lipid membranes are a different class of fluid surfaces which are, unlike other self-assembling media, highly flexible quasi-two-dimensional fluids, with their mechanics and thermodynamics being controlled by their bending energy since they are typically tensionless. They can readily deform to accommodate an adsorbed colloidal or nanoscale particle to a shape determined by the interplay between the adhesion of the particle on the lipid membrane and its curvature energy. Lipid membranes naturally serves as a medium for the assembly of a variety of biomolecules, including caveolin [5] and clathrin [6] and the Bin-Amphyphysin-Rvs (BAR) domain family of proteins [7–9].

Nanoparticles have many promising biomedical applications in biosensing [10], medical imaging [11], gene therapy [12], and treatment of cancer [13]. Meanwhile, there is an increasing concern in regard to the potential toxic effects of some nanoparticles on living organisms [14]. As a result, many studies have been conducted to investigate the interactions between single nanoscale particles with lipid membranes [15–20]. The pioneering work of Koltover *et al.* [21] demonstrated that 300 nm-900 nm spherical latex beads, which are adsorbed on giant unilamellar vesicles, self-assemble into linear chains or close-packed hexagonal structures. Saric and Cacciuto showed, using coarse-grained simulations of triangulated membranes, that the induced membrane curvature due to adhesion of spherical nanoparticles leads to their self-assembly into linear or hexagonally-packed aggregates [22]. Studies of the self-assembly of anisotropic nanoparticles on lipid membranes are however lacking.

In this article, we present a computational investigation of the interaction between elongated ad curved nanoparticles and lipid membranes and the ensuing self-assembly of the nanoparticles on the biomembrane. Specifically, we focus on elongated nanoparticles with a shape of a solid arc and square cross-section and with the inner face of the nanoparticle that interacts attractively with the lipid head groups. We will show that these nanoparticles create distinct self-assemblies that depend

*Submitted to Faraday Discussions on November 2, 2015
†Email: sunil@iitm.ac.in
‡Email: mlaradji@memphis.edu

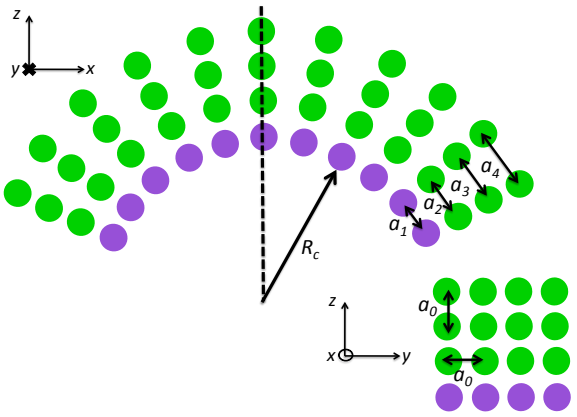

FIG. 1: Schematic representation of a longitudinal slice of an elongated nanoparticle along the xz-plane. Purple (n) beads interact attractively with the lipid head beads, while the green (p) beads interact repulsively with the lipid head beads. Both n and p beads interact repulsively with the lipid tail beads. A spontaneous curvature of the nanoparticle is induced by setting the preferred inter-particle separations to $a_1 < a_2 < a_3 < a_4$. A transverse slice of the nanoparticle along the yz-plane, shown by the dashed line, is displayed in the bottom right. Bond lengths in this plane are set to a_0.

on the adhesion strength. At low values of the adhesion strength, the nanoparticles arrange side-by-side creating linear chains. At high values of the adhesion strength, however, the nanoparticles self-assemble into aster clusters. These aster-shaped clusters can from a meshwork with triangular symmetry at large enough concentrations of nanoparticles.

II. MODEL

A mesoscale implicit-solvent model for lipid membranes is used here to study the self-assembly of anisotropically curved nanoparticles on lipid vesicles [23]. In this model, each lipid is coarse-grained into a semi-flexible linear chain composed of one head (h) bead and two (t) tail beads. Since the solvent in this model is implicit, the hydrophobic interactions that lead to the self-assembly of lipids is effectively accounted for by making $t-t$ interactions attractive.

As shown schematically in Fig. 1, each nanoparticle is modeled as a composite of two types of beads. The beads of the bottom layer (concave surface), labeled n, interact attractively with the lipid head beads while the remaining beads in the nanoparticle, labeled p, interact repulsively with the lipid beads. This favours the adhesion of the bottom layer of the nanoparticle on the lipid bilayer, as shown in Fig. 1. Within a nanoparticle, the beads are arranged in a distorted simple cubic lattice and nearest neighbour beads are linked by harmonic springs. The desired curvature of the nanoparticle is ensured by setting the rest length of the bonds a_1, a_2, a_3, and a_4 as shown in the Fig. 1.

The potential energy of the system is given by,

$$U\left(\{\mathbf{r}_i\}\right) = \sum_{i,j} U_0^{\alpha_i\alpha_j}\left(r_{ij}\right) + \sum_i \sum_{j\in\Omega_i} U_{\rm bond}^{\alpha_i\alpha_j}\left(r_{ij}\right) + \sum_i \sum_{k\in\Omega_i} \sum_{l\in\Omega_i} U_{\rm bend}^{\alpha_i}\left(\mathbf{r}_{ik},\mathbf{r}_{il}\right), \quad (1)$$

where $\mathbf{r}_i$ is the position of bead i and $r_{ij} = |\mathbf{r}_i - \mathbf{r}_j|$. The type of bead i, $\alpha_i = h$, t, n and p for a lipid head bead, lipid tail bead, a nanoparticle bottom layer bead, or other beads in the nanoparticle respectively. Ω_i is the set of beads bonded to bead i. In Eq. (1), $U_0^{\alpha_i\alpha_j}$ is a soft two-body interaction between beads i and j and is given by,

$$U_0^{\alpha_i\alpha_j}(r) = \begin{cases} (U_{\rm max}^{\alpha_i\alpha_j} - U_{\rm min}^{\alpha_i\alpha_j})\frac{(r_m-r)^2}{r_m^2} + U_{\rm min}^{\alpha_i\alpha_j} & \text{if} \quad r \le r_m, \\ -2U_{\rm min}^{\alpha_i\alpha_j}\frac{(r_c-r)^3}{(r_c-r_m)^3} + 3U_{\rm min}^{\alpha_i\alpha_j}\frac{(r_c-r)^2}{(r_c-r_m)^2} & \text{if} \quad r_m < r \le r_c, \\ 0 & \text{if} \quad r > r_c, \end{cases} \quad (2)$$

where $U_{\rm max}^{\alpha\beta} > 0$ for any pair (α,β). A negative value of $U_{\rm min}^{\alpha\beta}$ implies a short-range attraction between two beads of types α and β at intermediate distances. Except for $(\alpha,\beta) = (t,t)$ or $(\alpha,\beta) = (h,n)$, $U_{\rm min}^{\alpha\beta} = 0$ for any other interacting pair. A negative $U_{\rm min}^{tt}$ allows for the self-assembly of the lipid molecules into thermodynamically stable bilayers [23, 24], and a negative $U_{\rm min}^{hn}$ allows the nanoparticles to adhere to the lipid bilayer.

Beads that belong to a single lipid molecule or a nanoparticle are linked through $U_{\rm bond}^{\alpha\beta}$ given by

$$U_{\rm bond}^{\alpha_i\alpha_j}\left(r_{ij}\right) = \frac{k_{\rm bond}^{\alpha_i\alpha_j}}{2}(r_{ij} - a^{\alpha_i\alpha_j})^2, \quad (3)$$

where $k_{\rm bond}^{\alpha_i\alpha_j}$ and $a^{\alpha_i\alpha_j}$ are the stiffness and preferred

length of bond α_i-α_j, respectively.

In Eq. (1), $U^{\alpha}_{\rm bend}$ is the three-body interaction potential energy which provides stiffness to the lipids and nanoparticles and is given by,

$$U^{\alpha_i\alpha_k\alpha_l}_{\rm bend}(\mathbf{r}_{ik},\mathbf{r}_{kl}) = \frac{k^{\alpha_i\alpha_k\alpha_l}_{\rm bend}}{2}\left(\cos\theta^0_{\alpha_i\alpha_k\alpha_l} - \hat{\mathbf{r}}_{ik}\cdot\hat{\mathbf{r}}_{kl}\right)^2, \quad (4)$$

where $k^{\alpha_i\alpha_k\alpha_l}_{\rm bend}$ and $\theta^0_{\alpha_i\alpha_k\alpha_l}$ are the bending stiffness of a triplet $(\alpha_i,\alpha_k,\alpha_l)$ and its preferred splay angle, respectively.

In the present study, we set the interaction parameters $U^{tt}_{\rm min} = -6\epsilon$ and $U^{nh}_{\rm min} = -\xi$. Otherwise, we set $U^{\alpha_i\alpha_j}_{\rm min} = 0$. We also set $U^{tt}_{\rm max} = U^{nh}_{\rm max} = 200\epsilon$. Otherwise, $U^{\alpha_i\alpha_j}_{\rm max} = 100\epsilon$. For pairs of beads belonging to the same nanoparticle, we set $U^{nn}_{\rm min} = U^{pp}_{\rm min} = U^{pp}_{\rm min} = 0$, and $U^{nn}_{\rm max} = U^{pp}_{\rm max} = U^{pp}_{\rm max} = 0$. In order to prevent the nanoparticles from aggregating in the absence of lipid membranes, interactions between two beads belonging to different nanoparticles are fully repulsive. For these pairs of beads, we set $U^{nn}_{\rm min} = U^{pp}_{\rm min} = U^{pp}_{\rm min} = 0$ and $U^{nn}_{\rm max} = U^{pp}_{\rm max} = U^{pp}_{\rm max} = 100\epsilon$.

TABLE I: Tangential bond lengths a_1, a_2, a_3 and a_4 for the case of $R_c = 11r_m$ and $R_c = 7.5r_m$.

	$R_c = 7.5r_m$	$R_c = 11r_m$
a_1/r_m	0.70	0.75
a_2/r_m	0.85	0.83
a_3/r_m	1.00	0.92
a_4/r_m	1.15	1.00

The elastic coefficients of the two-body and three-body interactions for the lipids are set to $k^{ht}_{\rm bond} = k^{tt}_{\rm bond} = 100\epsilon/r_m^2$ and $k^{htt}_{\rm bend} = 100\epsilon$, respectively. The rest bond length for the lipids is set to $a^{ht} = a^{tt} = 0.7r_m$ and the preferred splay angle of a lipid chain is set to $\theta^0_{htt} = 180^{\rm o}$.

Each nanoparticle is made of 480 beads arranged in a distorted simple cubic lattice, having four layers each composed of 30×4 beads (see Fig. 1). Each bead is linked to its nearest neighbours by the bonding potential $U^{pp}_{\rm bond}$, $U^{np}_{\rm bond}$ or $U^{nn}_{\rm bond}$ in Eq. (3). The rigidity of the nanoparticle is maintained by the three-body potential $U_{\rm bend}$ with the angle $\theta^0_{\alpha_i\alpha_j\alpha_k} = 90^{\rm o}$ if i and k in the triplet are next nearest neighbours and $\theta^0_{\alpha_i\alpha_j\alpha_k} = 180^{\rm o}$ if i, j and k are collinear. In order to induce a radius of curvature R_c in the nanoparticle, the preferred bond lengths a along the longitudinal direction are set to values given in Table. I (see Fig. 1). Along the two other directions, the bond length is set to $a_0 = 1.0r_m$ (see Fig. 1). The elastic coefficients of the two-body and three-body interactions for the lipids are set to $k^{nn}_{\rm bond} = k^{pp}_{\rm bond} = k^{np}_{\rm bond} = 1000\epsilon/r_m^2$ and $k^{ppp}_{\rm bend} = k^{ppn}_{\rm bend} = k^{nnp}_{\rm bend} = k^{nun}_{\rm bend} = 1000\epsilon$, respectively. The desired radius of curvature, R_c, of the nanoparticle is set by the combined effects of the bending potential and the variation in bond length along the radial direction.

Beads are moved using a molecular dynamics scheme with a Langevin thermostat [25]:

$$\begin{aligned}\dot{\mathbf{r}}_i(t) &= \mathbf{v}_i(t), \text{ and}\\ m\dot{\mathbf{v}}_i(t) &= -\nabla_i U(\{\mathbf{r}_i\}) - \Gamma\mathbf{v}_i(t) + \sigma\boldsymbol{\Xi}_i(t), \quad (5)\end{aligned}$$

where m is the mass of a each bead (same for all beads), Γ is a bead's friction coefficient, and $\sigma\boldsymbol{\Xi}_i(t)$ is a random force originating from the heat bath. $\boldsymbol{\Xi}_i(t)$ obeys

$$\langle\boldsymbol{\Xi}_i(t)\rangle = 0, \quad (6)$$

$$\langle\Xi^{(\mu)}_i(t)\,\Xi^{(\nu)}_j(t')\rangle = \delta_{\mu\nu}\delta_{ij}\delta(t-t'), \quad (7)$$

with μ, $\nu = x$, y, or z. The dissipative and random forces are interrelated through the dissipation-fluctuation theorem, which leads to the relationship

$$\Gamma = \sigma^2/2k_{\rm B}T. \quad (8)$$

The equations of motion are numerically integrated using the velocity-Verlet algorithm with $\Gamma = \sqrt{6}m/\tau$ where the timescale $\tau = r_m(m/\epsilon)^{1/2}$ with r_m and ϵ being used as scales for length and energy respectively. To ensure that systems reach thermal equilibrium, the simulations were run for at least $10^7\Delta t$, with the time step $\Delta t = 0.01\tau$. The simulations are run at $k_{\rm B}T = 3\epsilon$, a temperature at which the bilayer is in the fluid phase [24]. The vesicles in the simulations are composed of 180 000 lipids, corresponding to a diameter of $130\,r_m$.

III. MEMBRANE-MEDIATED INTERACTION BETWEEN NANOPARTICLES

In order to understand the effect of lipid membranes on the effective interactions between anisotropically curved nanoparticles, we first performed simulations of two and three nanoparticles with intrinsic radius of curvature $R_c = 11r_m$ on vesicles of diameter $130\,r_m$ and for adhesion strengths $\xi = 1.0\epsilon$, 2ϵ, 3.0ϵ, 4.0ϵ, 5.0ϵ, and 6.0ϵ. In these simulations, to conserve time, the two or three nanoparticles are initially placed parallel to each other. Similar results are obtained when placed relatively far from each other. Resulting equilibrium configurations together with distributions of the splay angle, ϕ, between the nanoparticles are shown in Figs. 2(a) and (c). This figure shows that for $\xi = 1.0\epsilon$, the two nanoparticles lie side-by-side and are very close to each other. For $\xi = 2.0$ and 3.0ϵ also, the nanoparticles are parallel to each other, but are not as close to each other as in the case of $\xi = 1.0\epsilon$. The angle distribution for the case of $\xi = 1.0\epsilon$ (purple line in Fig. 2(b)) is very narrow and is peaked at a very small splay angle, $\phi \approx 3^{\rm o}$. However, the peak position is higher for $\xi = 2\epsilon$ and 3ϵ, and the width of the distribution increases with increasing the adhesion strength. This is evident in the corresponding distributions (black and red lines) in Figs. 2(b) and (d) which are peaked at a small angle around $\phi_{\rm max} = 5^{\rm o}$. The width

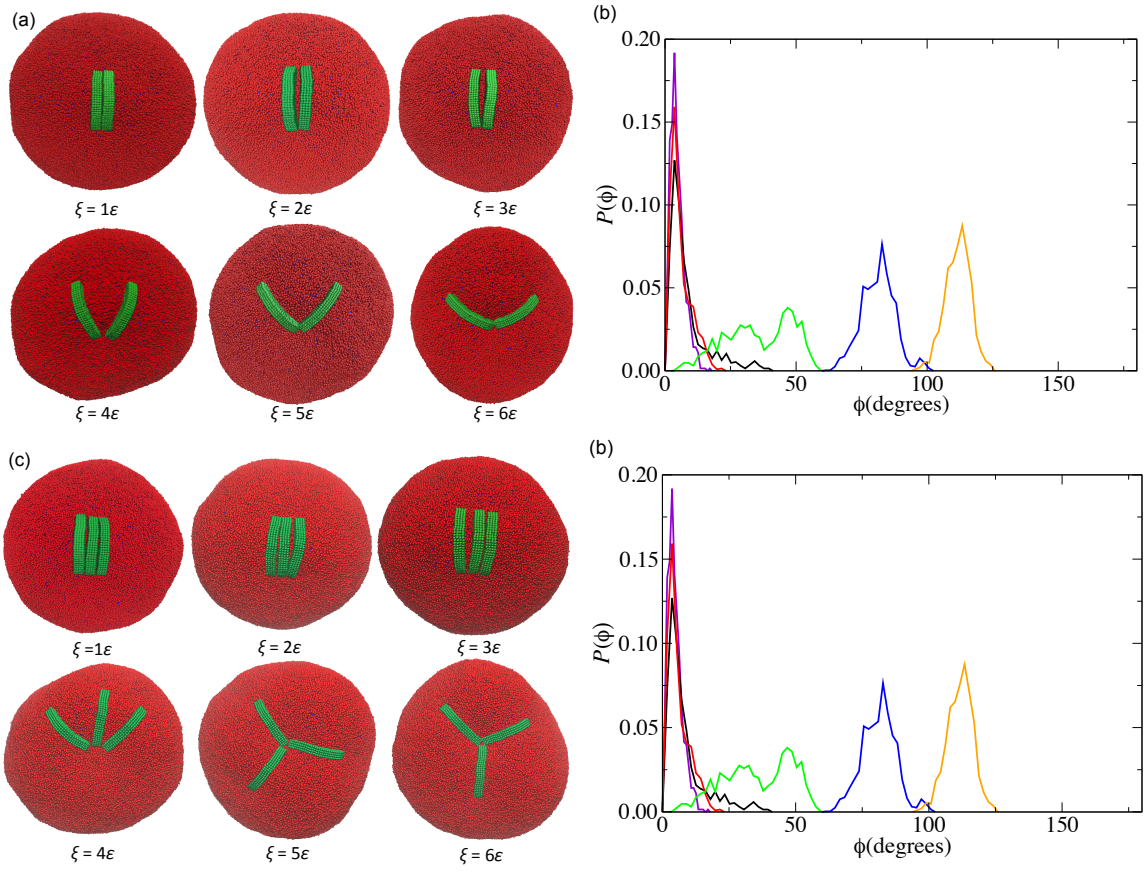

FIG. 2: (a) Equilibrium snapshots of lipid vesicles with two anisotropic nanoparticles having an intrinsic radius of curvature $R_c = 11r_m$ at adhesion strength ξ ranging between 1.0ϵ and 6.0ϵ. Green beads represent the nanoparticle and the red beads indicate the lipid head groups. (b) Splay angle distributions between two nanoparticles. Purple curve corresponds to $\xi = 1.0\epsilon$, red curve corresponds to $\xi = 2.0\epsilon$, black curve corresponds to $\xi = 3.0\epsilon$, green curve corresponds to $\xi = 4.0\epsilon$, blue curve corresponds to $\xi = 5.0\epsilon$, and the orange curve corresponds to $\xi = 6.0\epsilon$. (c) Same as in (a) but for three nanoparticles. (d) Same as in (b) for three nanoparticles with same colour coding.

of the distribution for $\xi = 3.0\epsilon$ is however higher than that for 2.0ϵ, implying that there is a tendency of the nanoparticles to splay from each other with increasing ξ. For $\xi \geq 4.0\epsilon$, the nanoparticles are clearly splayed from each as evident from both configurations and splay angle distributions with the preferred splay angle that increases with increasing the adhesion strength. It is noted that the splay angle between the nanoparticles is the result of membrane curvature mediated interactions and, for relatively high adhesion strength, it is influenced by the presence of other neighbouring nanoparticles as demonstrated by the configurations in Fig. 2(b) and the distributions of Fig. 2(d) which are broader and shifted for $\xi = 4.0$ and 5.0ϵ. This implies that at high adhesion strength, effective membrane-induced many-body interactions between the nanoparticles play an important role on their self-assembly.

We now turn to the question why a splay between the nanoparticles is induced at high adhesion strength. Since these conformations arise due to membrane mediated interactions a better understanding of the nature of membrane deformation induced by nanoparticles is necessary. We therefore performed simulations of a single nanoparticle with $R_c = 11r_m$ on a planar lipid bilayers for values of the adhesion strength varying between 1.0ϵ and 5.0ϵ. For all values of the adhesion strength considered here, the bilayer conforms to the curvature of the nanoparticle along its longitudinal direction. Profiles of the lipid bilayer at the plane transversally bisecting the nanoparticle at the midsection (dashed plane according to Fig. 1) are shown in Fig. 3 (c) and (d) at $\xi = 2.0\epsilon$ and $\xi = 5.0\epsilon$, respectively. This figure clearly shows that for $\xi = 2.0\epsilon$, the bilayer is not curved along the midsection plane of the nanoparticle. This implies that the nanoparticle locally induce positive mean curvature and zero Gaussian curvature of the bilayer. In contrast, for $\xi = 5\epsilon$, the bilayer is negatively curved in the midsection plane, while it is positively curved along the longitudinal direction. As a result, the nanoparticle locally induce a saddle profile of the lipid bilayer. This induced saddle region in the lipid bilayer must be due to the increased interaction between the lipid head groups and the bottom layer of

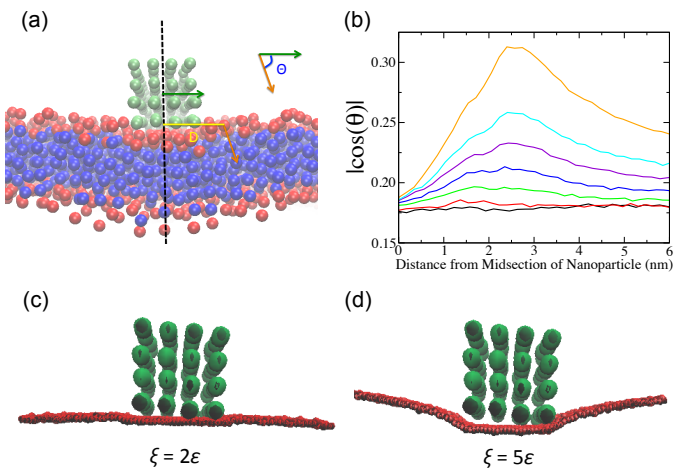

FIG. 3: (a) The cross section of a nanoparticle on a lipid bilayer. The yellow line represents the distance D of a lipid head particle from the median vertical plane bisecting the nanoparticle (shown by the black dashed line). The green vector is normal to the median plane and the orange vector is a typical head-to-tail vector for the lipid, with θ being the angle between them. (b) $|\cos(\theta)|$ vs D in the case of a nanoparticle with R_c=$11r_m$ bound to a $59r_m \times 59r_m$ lipid bilayer containing 10 000 lipids with constant lipid number density of $\rho = 3.20r_m^{-2}$. Only lipids in the top leaflet of the membrane and within a cutoff distance of $5r_m$ from the bottom layer of the nanoparticle are considered. In (b), curves from bottom to top, correspond to ξ=1.0ϵ, 1.5ϵ, 2.0ϵ, 2.5ϵ, 3.0ϵ, 4.0ϵ, and 5.0ϵ, respectively. (c) and (d) The height profile of the lipid bilayer, at the mid-section of the bound nanoparticle (yz-plane in Fig. 1) for the cases of $\xi = 2.0\epsilon$ and 5.0ϵ, respectively.

the nanoparticle.

The induced negative curvature of the bilayer in the midsection is further quantified by the relationship between the tilt of the lipids, defined as the angle between the horizontal and the end-to-end vector of a lipid, and their distance from the nanoparticle in the proximal leaflet at the midsection plane, as illustrated in Fig. 3(a). Fig. 3(b) shows that for $\xi = 1.0\epsilon$ and 1.5ϵ, $|\cos\theta| \approx 0.17$ implying an angle $\theta \approx 80^o$, independent of the distance between the lipids and the nanoparticle, which correspond to the horizontal membrane profile at the midsection plane of the nanoparticle, as clearly indicated by Fig. 3(c). This favours a side-by-side configuration, of the two nanoparticles. The low but finite values of $|\cos\theta|$ at these low adhesion strengths are due to thermal fluctuations. As the adhesion strength is increased, the $|\cos\theta|$ distribution shows a clear peak with the peak position shifting to the right. This clearly shows that the lipid tilt increases with increasing the adhesion strength and is maximum at the boundary of the nano particle. The resulting induced saddle deformation in the bilayer makes it difficult for another nanoparticle to be close and parallel to each other.

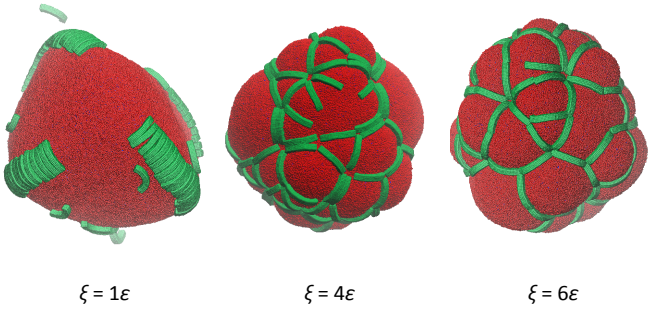

FIG. 4: Snapshots of 100 nanoparticles with intrinsic radius of curvature $R_c = 11r_m$ on a vesicles with diameter $130r_m$. Snapshots from left to right correspond to $\xi = 1.0\epsilon$, 4.0ϵ, and 6.0ϵ respectively. In the case of $\xi = 1.0\epsilon$, few nanoparticles are not bound to the vesicle or adheres sidewise to the membrane. This is due to the fact that the long chain clusters induce tension on the membrane which prevents the nanoparticles from generating local curvature and full binding. These nanoparticle will eventually fully bind after their diffusion to the ends of the chain clusters which are curvature friendly regions.

IV. SELF-ASSEMBLY

In order to investigate the nature of aggregation of the nanoparticles on a vesicle, we performed an extensive amount of simulations with 100, and 200 nanoparticles of radius of curvature $R_c = 11r_m$, on vesicles with diameter of $130\,r_m$. In the initial configurations, the nanoparticles are positioned and oriented randomly very close to the spherical lipid vesicles. In Fig. 4, snapshots are shown for the case of 100 nanoparticles with $\xi = 2.0\epsilon$, 4.0ϵ and 6.0ϵ. This figure clearly shows that the adhesion strength strongly affects the nature of self-assembly of the nanoparticles. At low values of adhesion strength ($\xi = 2.0\epsilon$), the nanoparticles are self-assembled in linear chains while in the case of high values of adhesion strength ($\xi = 4.0\epsilon$ and 6.0ϵ), the nanoparticles are arranged into asters with the average number of nanoparticles per aster increasing with ξ. These are in excellent agreement with the results presented above for two and three nanoparticles. The clear bulges, between the nanoparticles, in the vesicle for the case of $\xi = 6.0\epsilon$ are due to the saddle regions in the membrane created by the nanoparticles at high adhesion strength (see Fig. 3).

Effect of Nanoparticles Number Density on their Self-Assembly: We now turn to exploring the effect of the surface number density of the nanoparticles on their membrane-mediated self-assembly. Fig. 5 shows configurations of vesicles with $N = 100$ and 200 nanoparticles at $\xi = 2.0\epsilon$ and 6.0ϵ. In the case of $\xi = 2.0\epsilon$, chain-like aggregates are the dominant form of self-assembly. For $N = 200$, the chains intersect at triangular vertices and the average chain segment size is smaller than that for $N = 100$. These triangular clusters are defects that arise at high nanoparticles densities due to geometrical

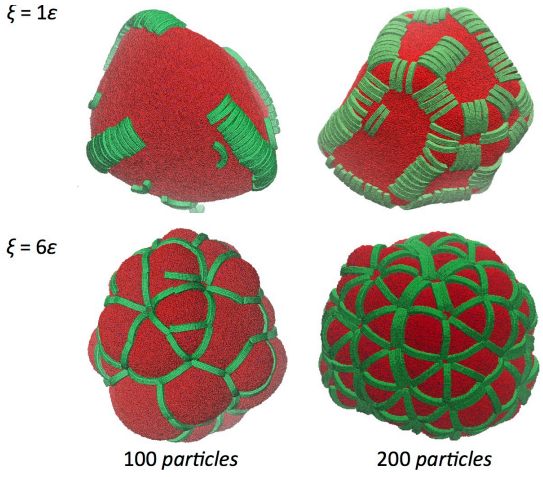

FIG. 5: Equilibrium snapshots of lipid vesicles with 100, and 200 nanoparticles (left to right) and intrinsic radius of curvature $R_c = 11r_m$, and at adhesion strengths $\xi = 1.0\epsilon$ (top row) and 6.0ϵ (bottom row).

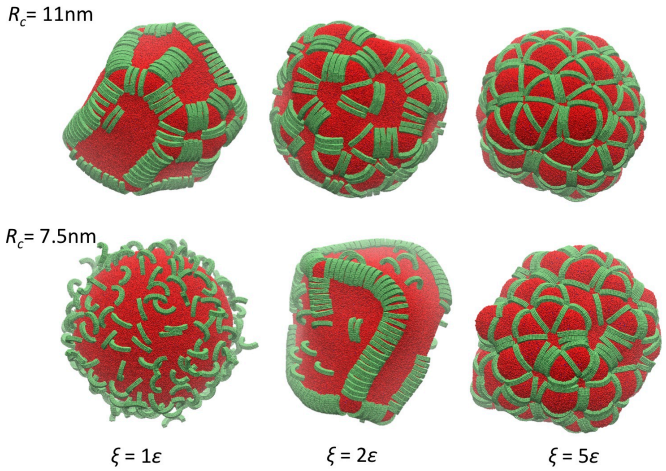

FIG. 6: Equilibrium snapshots 200 nanoparticles with intrinsic radius of curvature $R_c = 11r_m$ (top row) or $R_c = 7.5r_m$ (bottom row) and adhesion strengths $\xi = 1.0\epsilon$ (left column), 2.0ϵ (center column) and 5.0ϵ (right column).

constraints induced by the finite spherical surface.

For $\xi = 6.0\epsilon$, the splay angles between neighbouring nanoparticles for the case of $N = 100$ are clearly larger in average that those for the case of $N = 200$. In fact, for $N = 200$, most of the the splay angles between neighbouring particles are about 60°, which is a result of the fact that a large number of nanoparticles cannot be self-assembled onto the vesicle with large splay angles as in the case of $N = 100$. The asters for the case of $N = 200$ have a somewhat hexagonal symmetry and form a meshwork spanning the whole vesicle. In this case, even though $\xi = 6.0\epsilon$ is high, crowding effects lead some nanoparticles to be arranged side-by-side, a situation that does not occur at low number density is low ($N = 100$).

Effect of Nanoparticle Curvature: We extended our study to also investigate the effect of the nanoparticles intrinsic radius of curvature, R_c. In Fig. 6, equilibrium configurations of vesicles with $N = 200$ nanoparticles for $R_c = 7.5r_m$ and $11r_m$ are shown for $\xi = 1.0\epsilon$, 2.0ϵ and 6.0ϵ. This figure shows that the weakly curved nanoparticles ($R_c = 11r_m$) are all bound to the membrane and self-assembled into chains at $\xi = 1.0\epsilon$. In contrast, none of the highly curved ($R_c = 7.5r_m$) nanoparticles are not fully bound to the vesicle and few are only adsorbed to the vesicle by their two ends. This is due to the fact for $R_c = 7.5r_m$ and at low values of ξ, the gain in free energy through full adhesion of the nanoparticles to the vesicle is not enough to compensate for the loss in energy resulting from bending the lipid bilayer. At $\xi = 2.0\epsilon$, the weakly curved nanoparticles ($R_c = 11r_m$) self-assemble into chains, albeit with an average size that is shorter than that for $\xi = 1.0\epsilon$. The highly curved nanoparticles, at the same adhesion strength, however are self-assembled into chains that are in average longer than for the case of $R_c = 11r_m$ at $\xi = 1.0\epsilon$. It is interesting to note that few of the highly curved nanoparticles at $\xi = 2.0\epsilon$ are merely adsorbed by their two ends. These monomeric nanoparticles cannot easily fully bind to their inability to generate local curvature of the membrane because of the tension induced on the membrane by the long fully bound chains.

V. CONCLUSION

In conclusion, we presented in this article a large scale study of the self-assembly of anisotropically curved nanoparticles on lipid vesicles via coarse-grained molecular dynamics simulations of an implicit-solvent model. Our simulations show that the curved nanoparticles are able to generate a local curvature of the membrane which then mediates their self-assembly into either chains or asters. Chains, in which the nanoparticles are arranged side-by-side are formed at weak adhesion strength. As the adhesion strength increases, the nanoparticles induce saddle curvature deformations on the membrane which results in aster aggregates to emerge. At high surface densities of the nanoparticles the effect of tension, induced by binding of the curvature-generating nanoparticles, also affect the binding affinity of the particles and plays a role in determining the type of self-assembly. In particular, the aster clusters tend to be isolated and have a small number of arms for small densities, while at high densities, the asters form a meshwork with hexagonal symmetry. We hope that the present study will incite future experiments on the self-assembly of anisotropically curved nanoparticles on lipid membranes. Crescent-shaped gold nanoparticles [26–28] with appropriate functionalization should be a good candidate to perform such

experiments.

Acknowledgements

This work was supported by the National Science Foundation (DMR-0812470), the National Institute of General Medical Sciences of NIH (R15GM106326), the American Physical Society Travel Grant Program, and a Faculty Research Grant from the University of Memphis. The later support does not necessarily imply endorsement by the University of research conclusions. All simulations were performed on computers of the High Performance Computing Facility of the University of Memphis.

[1] X. Zeng, F. Liu, A.G. Fowler, G. Ungar, L. Cseh, G.H. Mehl, and J.E. MacDonaldAdv. Mater. **21**, 1746 (2009).
[2] W.A. Lopes and H.M. Jaeger, Nature **414**, 735 (2001).
[3] Z. Niu, J. He, T.P. Russel, and Q. Wang, Angew. Chem. Int. Ed. **49**, 10052 (2010).
[4] M.J.A. Hore and M. Laradji, J. Chem. Phys. **126**, 244903 (2007).
[5] I. Fernandez, Y. Ying, J. Albanesi, and R.G.W. Anderson, Proc. Nat. Acad. Sci. USA **99**, 11193 (2002).
[6] R. Matthews, and C.N. Likos, Soft Matter **9**, 5794 (2013).
[7] A. Frost, R. Perera, A. Roux, K. Spasov, O. Destaing, E. H. Egelman, P. De Camilli, and V. M. Unger, Cell **132**, 807 (2008).
[8] B. J. Peter, H. M. Kent, I. G. Mills, Y. Vallis, P. J. G. Butler, et al., Science **303**,495 (2004).
[9] M. G. Ford, I. G. Mills, B. J. Peter, Y. Vallis, G. J. Praefcke, et al., Nature **419**, 361 (2002).
[10] S.T. Selvan, T.T.Y. Tan, D.K. Yi, and N.R. Jana, Langmuir **26**, 11631-11641 (2010).
[11] J.L. West and N.J. Hala, Annu. Rev. Biomed. Eng. **5**, 285-292 (2003).
[12] M.E. Davis, J.E. Zuckermann, C.H.J. Choi, D. Seligson, A. Tolcher, C.A. Alabi, Y. Yen, J.D. Heidel, and A. Ribas, Nature **464**, 1067 (2010).
[13] K.K. Jain, Technol. Cancer Res. TReat. **4**, 407-416 (2005).
[14] N. Lewinski, V. Colvin, and R. Drezek, Small **4**, 26 (2008).
[15] O. Le Bihan, P. Bonnafous, L. Marak, T. Bickel, S. Trépout, S. Mornet, F. De Haas, H. Talbot, J.-C. Taveau, and O. Lambert, J. Struct. Biol. **168**, 419-425 (2009).
[16] M. Deserno and T. Bickel, Europhys. Lett. **62**, 767-773 (2003).
[17] T. Ruiz-Herrero, E. Velasco, and M.F. Hagan, J. Phys. Chem. B **116**, 9595 (2012).
[18] X. Yi and H. Gao, Soft Matter **11**, 1107-1115 (2015).
[19] S. Dasgupta, T. Auth, and G. Gompper, Nano Lett. **14**, 687-693 (2014).
[20] R. Vácha, F.J. Martinez-Veracoechea, and D. Frenkel, Nano Lett. **11**, 5391-5395 (2011).
[21] I. Koltover, J.O. Rädler, and C.R. Safinya, Phys. Rev. Lett. **82**, 1991 (1999).
[22] A. Saric and A. Cacciuto, Phys. Rev. Lett. **108**, 118101 (2012).
[23] Joel D. Revalee, Mohamed Laradji, P. B. Sunil Kumar, J. Chem. Phys. **128**, 035102, (2008).
[24] E.J. Spangler, P. B. Sunil Kumar, Mohamed Laradji, Soft Matter **8**, 10896 (2012).
[25] G. S. Grest and K. Kremer, Phys. Rev. A **33**, 3628 (1986).
[26] J.S. Shumaker-Parrt, H. Rochholz, and M. Kreiter, Adv. Mater. **17**, 2131 (2005).
[27] H. Rochholz, N. Bocchio, and M. Kreiter, New J. Phys. **9**, 53 (2007).
[28] A. Unger, U. Rietzler, R. Berger, and M. Kreiter, NanoLett. **9**, 2311 (2009).